biology

MDPI

Article

In Vivo Hepatoprotective and Nephroprotective Activity of Acylated Iridoid Glycosides from *Scrophularia hepericifolia*

Maged S. Abdel-Kader [1,2,*] and Saleh I. Alqasoumi [3]

[1] Department of Pharmacognosy, College of Pharmacy, Prince Sattam Bin Abdulaziz University, Al-Kharj 11942, Saudi Arabia
[2] Department of Pharmacognosy, College of Pharmacy, Alexandria University, Alexandria 21215, Egypt
[3] Department of Pharmacognosy, College of Pharmacy, King Saud University, Riyadh 11451, Saudi Arabia; sqasoumi@ksu.edu.sa
* Correspondence: mpharm101@hotmail.com; Tel.: +966-545-539-145

Simple Summary: Chronic liver disease is a major life-threating problem worldwide. Deaths due to liver disease constituted 2.4% of total deaths globally in 2017. Yet most of the available drugs for improving liver conditions are of natural origin. More research is necessary to discover agents that are more effective. Previously, the extract of *Scrophularia hypericifolia* showed promising protection of liver and kidney tissues against induced toxicity in experimental animals. The current phytochemical study aimed to identify the active molecules in the extract. Nine iridoid glycoside derivatives were identified from the plant extract, including four new compounds after extensive chromatographic purification. The structures were identified by applying various spectroscopic methods. Biological evaluation for protective effect on liver and kidney tissues was conducted on compounds isolated with a high enough yield. Serum and tissue parameters as well as histopathological studies were conducted for efficacy evaluation. Two of the new compounds showed the best protection of liver and kidney tissues as indicated by the studied parameters. These findings indicated that natural products could provide solutions to health problems. The role of nutraceuticals in managing liver problems is a promising field for further studies.

Abstract: Phytochemical investigation of the chloroform fraction obtained from *Scrophularia hypericifolia* aerial parts led to the isolation of nine acylated iridoid glycosides. The new compounds were identified as 6-O-α-L(2″-acetyl, 3″,4″-di-O-*trans*-cinnamoyl) rhamnopyranosyl-6′-acetyl catalpol (6′-acetyl hypericifolin A) (**1**), 6-O-α-L(2″, 4″-diacetyl, 3″-O-*trans*-cinnamoyl) rhamnopyranosyl-6′-acetyl catalpol (6′-acetyl hypericifolin B) (**2**), 6-O-α-L(2″-acetyl, 3″,4″-di-O-*trans*-cinnamoyl) rhamnopyranosyl catalpol (hypericifolin A) (**3**) and 6-O-α-L(2″, 4″-diacetyl, 3″-O-*trans*-cinnamoyl) rhamnopyranosyl catalpol (hypericifolin B) (**4**). Previously reported compounds were identified as laterioside (**5**), 8-O-acetylharpagide (**6**), 6-O-α-L(4′-O-*trans*-cinnamoyl) rhamnopyranosyl catalpol (**7**), lagotisoside D (**8**) and harpagoside (**9**). Identification achieved via analyses of physical and spectral data including 1D, 2D NMR and High Resolution Electrospray Ionization Mass spectroscopy (HRESIMS). Compounds **2**–**4** and **6** were subjected to biological evaluation against paracetamol-induced toxicity. The biochemical parameters aspartate aminotransferase (AST), alanine aminotransferase (ALT), alkaline phosphatase (ALP) and gamma glutamyl transpeptidase (GGT) as well as total bilirubin were used to access the liver condition. Measurement of serum levels of urea, creatinine, sodium and potassium cations were indicators for kidney condition. Liver and kidney samples were subjected to histopathological study. The best protection was found in the group treated with **3** followed by **4** and **6**, while **2** was almost inactive.

Keywords: *Scrophularia hypericifolia*; acylate iridoid glycoside; hepatoprotective; nephroprotective

Citation: Abdel-Kader, M.S.; Alqasoumi, S.I. In Vivo Hepatoprotective and Nephroprotective Activity of Acylated Iridoid Glycosides from *Scrophularia hepericifolia*. *Biology* **2021**, *10*, 145. https://doi.org/10.3390/biology10020145

Academic Editor: Xuehong Zhang

Received: 6 January 2021
Accepted: 6 February 2021
Published: 12 February 2021

1. Introduction

The genus *Scrophularia* consists of 200–300 species, present mainly in Asia, Europe and, to a lesser extent, North America [1]. Only four species of the genus *Scrophularia* are present in Saudi Arabia [2,3]. Members of this genus are used traditionally as anti-inflammatory, anticancer, laxative, diuretic, heart and circulatory stimulant treatments [4,5]. They are also applied for the treatment of pharyngitis, neuritis, laryngitis, smallpox, measles, high-heat plague and poisoning, dermatitis and rheumatoid arthritis [4,6,7]. Pharmacological studies revealed that members of the genus possess antibacterial, antioxidant [8], anti-inflammatory, antidiabetic [9], cardioprotective [10], hepatoprotective, immunostimulant [11,12], wound healing [13] and insecticidal [14] activities.

Scrophularia species are rich in iridoid glycosides. The hepatoprotective effect of *S. koelzii* was traced to the iridoid glycosides scropolioside A, harpagoside and koelzioside [12]. Scropolioside D2 and harpagoside B isolated from *S. deserti* showed significant anti-inflammatory and antidiabetic effects [9]. Iridoid glycosides from *S. umbrosa* were reported to have inhibitory activity on nitric oxide production [15]. Two iridoid glycosides with analgesic activity were reported from *S. kotscyhana* [16].

Chronic liver diseases are one of the major causes of morbidity and mortality globally. In 2017, liver diseases caused more than 1.32 million deaths in females and 883,000 in males, compared with less than 899,000 deaths in 1990 worldwide. Deaths due to liver disease constituted 2.4% of total deaths globally in 2017 compared with 1.9% in 1990 [17]. Non-alcoholic fatty liver disease (NAFLD) is characterized by inflammation and progressive tissue degeneration. It affects about 5% of the general adult population, and 20% of obese people [18]. In the absence of specific approved drugs on the market for the treatment of NAFLD, some nutraceuticals could contribute to the improvement of lipid infiltration and/or biochemical parameters. A few nutraceuticals were studied clinically for their effects against NAFLD, including silymarin (Sil), vitamins E and D, curcumin, resveratrol and the total extracts of *Salvia milthiorriza* [19].

Scrophularia hypericifolia growing in Saudi Arabia was reported to have hepatoprotective and nephroprotective activities [20]. In the current study, the secondary metabolites of the plant were isolated and identified by various spectroscopic methods. Pure compounds isolated in good yield were evaluated for their hepatoprotective and nephroprotective activities.

2. Results and Discussion

2.1. Structure Elucidation

The total extract of the aerial parts of *S. hypericifolia* was partitioned by liquid–liquid fractionation to a petroleum ether-soluble fraction, chloroform-soluble fraction and n-butanol-soluble fraction. Extensive chromatographic fractionation and purification of the chloroform-soluble fraction resulted in the isolation of compounds **1**–**9** (Figure 1) in addition to cinnamic acid. The known compounds were identified by comparison of their measured spectra with the literature data. All the assignments of ^{1}H and ^{13}C values were based on DEPT135, COSY, HSQC, HMBC, H2BC, NOESY and/or ROESY experiments. Compound **5** was identified as laterioside, an iridoid glycoside first identified from *S. lateriflora* [21] then reported from *S. deserti* [22] as well as many *Verbascum* species [23]. Compound **6** was identified as 8-O-acetylharpagide common in *Scrophularia* species [24]. 8-O-Acetylharpagide is reported to have antibacterial, anti-inflammatory, vasoconstrictor and cancer chemopreventive activities [25–28]. Compound **7** was identified as 6-O-α-L(4″-O-*trans*-cinnamoyl) rhamnopyranosyl catalpol. Compound **7** is reported in this work for the first time from *Scrophularia* species. Previously, it was characterized from *Gmelina arborea* (Lamiaceae) and *Buddleja polystachya* (Scrophulariaceae) [29,30]. The data of **8** enable the identification of the structure as lagotisoside D previously isolated from *Lagotis yunnanensis* and *S. dentata* [31,32]. Compound **9** data were identical to those reported for harpagoside [33]. Harpagoside was first isolated from *Harpagophytum procumbens* F. Pedaliaceae

(devil's claw) [34]. Harpagoside proved to have potent anti-rheumatic, anti-inflammatory and analgesic effects [35].

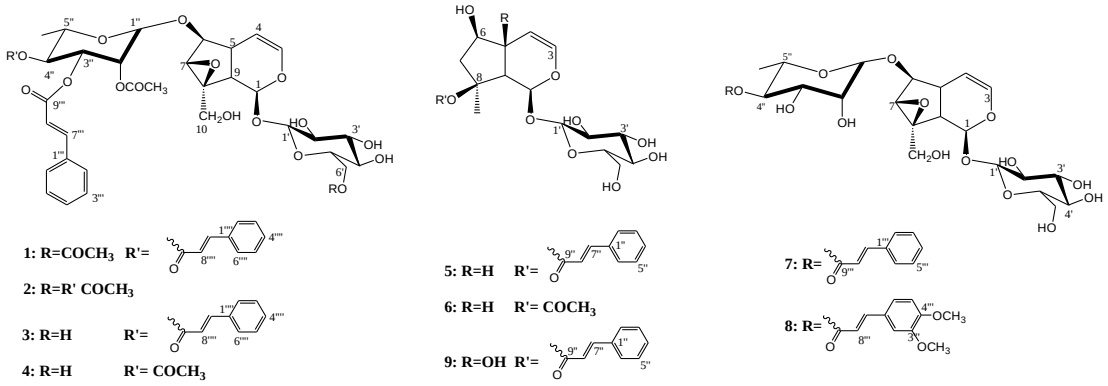

Figure 1. Structures of the isolated compounds (**1**–**9**).

The HRESIMS of **1** showed an $[M+Na]^+$ m/z of 875.2733 and $[M+K]^+$ m/z of 891.2471 for the molecular formula $C_{43}H_{48}O_{18}$ (Figures S20 and S21). The ^1H and ^{13}C NMR data of **1** (Tables 1 and 2) indicated the presence of two acetyl moieties at δ_H 2.07, δ_C 19.54, 171.40; δ_H 2.19, δ_C 19.48, 170.32 and two *trans*-cinnamoyl moieties as indicated by two conjugated ester carbonyls at δ_C 165.93, 166.31 and the *trans*-coupled protons at δ_H 6.40, 6.50, 7.61, 7.70 (each d, J = 16 Hz) along with the overlapped aromatic protons at δ_H 7.35, 7.49 and 7.53 (Figures S1–S7). ^{13}C NMR of **1** showed ten carbon resonances sorted by DEPT 135 experiments into 7 X CH including two oxygenated, two vinyls and one di-oxygenated methins, one CH_2O and one oxygenated quaternary carbon. Such an array (Tables 1 and 2) pointed to an iridoid skeleton of a catalpol skeleton [36]. Another set of carbons, including four CHO, CH_2O and one di-oxygenated CH were assigned to glucose moiety attached to C-1 of the iridoid aglycone. The relative stereochemistry of the iridoid aglycone was confirmed from the NOE correlations between the protons H-1 and H-6; H-6 and H-7; H-6 and H-10, all with α-orientation (Figures S17–S20). The chemical shift of C-6 at δ_C 83.74 was diagnostic for a substituted position. The six carbon resonances at δ_C 96.41, 71.05, 69.92, 69.45, 66.89 in addition to the methyl carbon at δ_C 16.53 correlated by the HSQC experiment with the proton doublets at δ_C 1.27 in ^1H NMR spectra were assigned to a rhamnosyl substituent (Figure S9). HMBC correlations between the H-6 doublet at δ_H 4.03 and C-1′′ of rhamnose at δ_C 96.41δ_C as well as the NOE correlation between H-6 and H-1′′ singlet at δ_H 5.13 all support the position of a rhamnosy moeity at C-6. Many iridoid glycosides including **7** and **8** bearing a rhamnose moiety at C-6 were previously reported (Figures S10–S14) [29–32]. Compared with compound **7**, **1** bears an additional two acetyls and one *trans*-cinnamoyl (Tables 1 and 2). The H-6′ and C-6′ of the glucose moiety in **1** were downfield shifted to δ_H 4.28 (dd, J = 5, 12 Hz), 4.47(d, J = 6.8 Hz) and δ_C 62.74 compared with normal values of glucose [33], indicating acylation at that position. NOE correlations were observed between the acetyl protons at δ_H 2.07 (s) and H-6′ at δ_H 4.28 (dd, J = 5, 12 Hz), 4.47(d, J = 6.8 Hz), H-5′ at δ_H 3.52 (m) and H-4′ at 3.43 (m) (Figures S17–S20). Further evidence for C-6′ acetylation was obtained from the HMBC correlations between both H-6′ protons, and the methyl protons at δ_H 2.07 with the acetyl carbonyl at δ_C 171.40 (Figures S10–S14). The H2BC experiment was extensively used to assign protons and carbons, especially those of the rhamnose moiety (Figures S15 and S16). The chemical shifts of H-2′′, H-3′′, H-4′′ at δ_H 5.43 (bs), 5.53 (dd, J = 2.7, 10 Hz) and 5.32 (t, J = 10 Hz) indicated that the three positions are acylated. The assignments of the two cinnamoyl and the left acetyl substituents to their exact positions on C-2′′-C4′′ were achieved via detailed analyses of the HMBC correlations. The broad singlet assigned for H-2′′ at δ_H 5.43 as well as the acetyl methyl singlet at δ_H 2.19 showed three bond correlations with the acetyl carbonyl at δ_C 170.32. HMBC correlations were observed between H-3′′ at 5.53 (dd, J = 2.7, 10 Hz), the two *trans*-oriented cinnamoyl doublets at δ_H 6.40 and 7.61 and the carbonyl signal at

δ_C 165.93 assigned to C-9‴, while the H-4″ triplet at δ_H 5.32, and the two *trans*-oriented cinnamoyl doublets at δ_H 6.50 and 7.70 were correlated to the carbonyl signal at δ_C 166.31 assigned to C-9⁗ (Figures S10–S14). Based on the provided evidence, **1** was identified as 6-O-α-L(2″-acetyl, 3″,4″-di-O-trans-cinnamoyl) rhamnopyranosyl-6′-acetyl catalpol and was given the name 6′-acetyl hypericifolioside A.

The HRESIMS of **3** showed an $[M+Na]^+$ m/z of 833.2616 and $[M+K]^+$ m/z of 849.2348 for the molecular formula $C_{41}H_{46}O_{17}$, indicating one acetyl group less than **1** (Figures S80 and S81). The appearance of H-6′ and C-6′ of glucose at δ_H 3.67 (dd, *J* = 6.5, 11.9 Hz), 3.96 (d, *J* = 10.9 Hz) and δ_C 61.58 in **3** indicated that C-6′ hydroxyl is free (Figures S50–S55). Spectra of **3** were repeated in pyridine-d6 to resolve overlapping peaks in the CD_3OD spectra, such as H-1, H-4 and H-1″ (Table 1) (Figures S66–S70). The assignment of the two cinnamoyl moieties at 3″, 4″ and the acetyl group at 2″ of the rhamnose moiety followed the same spectral evidence explained for **1**. The broad singlet assigned for H-2″ at δ_H 5.43 as well as the acetyl methyl singlet at δ_H 2.19 showed three bond correlations with the acetyl carbonyl at δ_C 170.31. HMBC correlations were observed between H-3″ at δ_H 5.55 (dd, *J* = 3.2, 10.2 Hz), the two *trans*-oriented cinnamoyl doublets at δ_H 6.39 and 7.60 and the carbonyl signal at δ_C 165.89 assigned to C-9‴, while the H-4″ triplet at δ_H 5.33 and the two *trans*-oriented cinnamoyl doublets at δ_H 6.49 and 7.71 correlated to the carbonyl signal at δ_C 166.30 assigned to C-9⁗ (Figures S58–S60 and S106). Consequently, **3** was identified as 6-O-α-L(2″-acetyl, 3″,4″-di-O-*trans*-cinnamoyl) rhamnopyranosyl catalpol and was given the trivial name hypericifolioside A.

Similar to **1** and **3**, the spectra of **2** pointed out a catalpol skeleton with a C-6 rhamnosyl substituent. The ^1H and ^{13}C NMR data of **2** (Tables 1 and 2) (Figures S23–S27) indicated the presence of three acetyl moieties at δ_H 2.00, δ_C 20.94, 170.72; δ_H 2.02, δ_C 21.07, 170.32; δ_H 2.13, δ_C 21.04, 170.06 and one *trans*-cinnamoyl moiety, as indicated by the conjugated ester carbonyls at δ_C 165.75 and the *trans*-coupled protons at δ_H 6.54, 7.60 (each d, *J* = 16 Hz) along with the aromatic protons at δ_H 7.43, 7.69. HRESIMS of **2** were in full support of the suggested structure, where it showed an $[M+Na]^+$ m/z of 787.2412 and $[M-1]^-$ m/z of 763.2454 for the molecular formula $C_{36}H_{44}O_{18}$ (Figures S48 and S49). This spectral evidence indicated that **2** has three acetyl groups over the structure of **7**. The H-6′ and C-6′ of glucose were downfield shifted to δ_H 4.14 (m), 4.31(m); δ_C 63.27 (DMSO), δ_H 4.69 (dd, *J* = 3.7, 11.4 Hz), 4.88 (d, *J* = 11.4 Hz) and δ_C 63.61 (pyridine-d6) (Figures S38–S42) compared with normal values of glucose [34]. This downfield shift supports C-6′ acetylation. More evidence for C-6′ acetylation was obtained from NOESY experiments where NOE correlations were observed between the acetyl protons at δ_H 2.00 (s) and H-5′ at δ_H 3.99 (m) (Figures S33–S37). An H2BC experiment was applied to assign the rhamnose protons and carbons (Figures S31 and S32). The downfield shift of H-2″, H-3″, H-4″ to δ_H 5.91 (s), 5.95 (d, *J* = 7.7 Hz) and 5.71 (t, *J* = 9.6 Hz) (pyridine-d6) (Figures S38 and S39) pointed out their acylated nature. The position of the cinnamoyl moiety was decided through the analysis of HMBC experiment correlations measured in pyridine d6 (Figures S44 and S45). Three bond contours were clear between H-3″ at δ_H 5.95 and the cinnamoyl carbonyl signal at δ_C 165.89. Both H-2″, H-4″ at δ_H 5.91, 5.71 showed three bond correlations with the two acetyl carbonyls at δ_C 169.89 and 170.21 (Figures S44 and S45). Based on the above discussion, compound **2** was identified as 6-O-α-L (2″, 4″-diacetyl, 3″-O-*trans*-cinnamoyl) rhamnopyranosyl-6′-acetyl catalpol and was given the trivial name 6′-acetyl hypericifolioside B.

Table 1. ^{1}H NMR data (δ ppm, *J* in parentheses in Hz) for compounds 1–4 and 7 *.

Pos.	1	2		3		4		7
	CD_3OD	DMSO d_6	Pyridine d_6	CD_3OD	Pyridine d_6	CD_3OD	Pyridine d_6	CD_3OD
1	4.95 (d, 9.8)	4.83 (d, 9.2)	5.45 **	5.14 **	5.51 (d, 8.8)	5.11 **	5.48 **	5.11 **
3	6.43 (d, 5.8)	6.44 (d, 1.5)	6.47 (d, 5.2)	6.43 (bd, 5.5)	6.48 (d, 5.7)	6.42 (bd, 6.0)	6.45 (d, 4.7)	6.41 (d, 5.7)
4	5.16 (t, 5.4)	5.04 **	5.45 **	5.14 **	5.19 (t, 5.0)	5.11 **	5.12 **	5.11 **
5	2.54 (bq, 4.5)	2.39 (bs)	2.76 (bs)	2.55 (bq, 4.3)	2.76 (bq, 3.9)	2.51 (bq, 4.6)	2.73 (bs)	2.45 (bq, 4.4)
6	4.03 (d, 8.0)	3.93 **	4.25 **	4.11 (d, 8.0)	4.12 **	4.09 (d, 8.4)	4.07 (d, 7.6)	4.05 (d, 8.1)
7	3.71 (s)	3.69 (s)	3.93 (s)	3.72 (s)	3.80 (s)	3.70 (s)	3.77 (s)	3.69 (s)
9	2.65 (t, 9.0)	2.46 (bt, 8.0)	2.85 (t, 7.7)	2.64 (t, 9.4)	2.84 (t, 8.9)	2.62 (bt, 9.3)	2.82 (bt, 8.0)	2.60 (t, 8.0)
10	3.78 (d, 13.0) 4.18 **	3.63 (d, 12.4) 3.93 **	4.39 (d, 13.0) 4.50 (d, 13.0)	3.87 (d, 13.2) 4.16 (m)	4.48 **	3.85 (d, 13.2) 4.18 (d, 13.2)	4.47 (s)	3.85 ** 4.18 (d, 13.2)
1′	4.83 (d, 7.9)	4.66 (d, 7.0)	5.45 (Overl.)	4.83 (d, 7.9)	5.51 (d, 8.8)	4.80 (d, 7.9)	5.48 **	4.80 (d, 7.9)
2′	3.32 (m)	3.11 (bt, 7.5)	4.10 (m)	3.32 (m)	4.12 **	3.28 (m)	4.14 (t, 7.8)	3.30 (m)
3′	3.43 (m)	3.25 (bt, 8.4)	4.25 **	3.46 (t, 9.0)	4.30 **	3.44 (bt,9.0)	4.07 (d, 7.6)	3.43 (q, 8.9)
4′	3.43 (m)	3.19 (bt, 8.9)	4.10 (m)	3.32 (m)	4.19 (bt, 9.2)	3.28 (m)	4.20 (t, 8.7)	3.30 (m)
5′	3.52 (m)	3.42 (m)	3.99 (m)	3.37 (m)	4.01 (bt, 6.7)	3.33 (m)	4.00 (bs)	3.30 (m)
6′	4.28 (dd, 5.0, 12.0) 4.47 (d, 6.8)	4.14 (m) 4.31 (m)	4.69 (dd, 3.7, 11.4) 4.88 (d, 11.4)	3.67 (dd, 6.5, 11.9) 3.96 (d, 10.9)	4.30 ** 4.53 (d, 11.8)	3.65 (dd, 6.8, 12.0) 3.94 (bd, 12.0)	4.30 ** 4.53 (d, 10.7)	3.67 ** 3.93 **
1″	5.13 (s)	5.14 (s)	5.45 **	5.14 **	5.43 (s)	5.11 **	5.38 (s)	5.03 (s)
2″	5.43 (bs)	5.27 (bs)	5.91(s)	5.43 (bs)	5.94 **	5.39 (m)	5.88 (s)	3.96 (m)
3″	5.53 (dd, 2.7,10.0)	5.27 (bs)	5.95 (d, 7.7)	5.55 (dd, 3.2, 10.2)	6.09 (dd, 2.6, 10.0)	5.41 (m)	5.94 (bd, 9.7)	3.96 (m)
4″	5.32 (t, 10.0)	5.04 **	5.71 (t, 9.6)	5.33 (t, 10.0)	5.89 **	5.17 (t, 9.8)	5.71 (t, 9.7)	5.11 **
5″	4.18 **	3.93 **	4.34 (m)	4.16 **	4.44 (m)	4.06 (m)	4.30 **	3.67 **
6″	1.27 (d, 6.0)	1.16 (d, 4.3)	1.38(d, 5.5)	1.28 (d, 6.2)	1.46(d, 6.0)	1.24 (d, 6.3)	1.37 (d, 5.4)	1.20 (d, 6.4)
3‴–5‴	7.35 **	7.43 (bs),	7.30 (bs),	7.34 **	7.31 (bs)	7.43 (m, 3H),	7.20- 7.57 **	7.43 (bs)
2‴, 6‴	7.49 (d, 6.6)	7.69 (bs)	7.47 (d, 5.8)	7.47 (d, 6.4)	7.24 (d, 7.3)	7.61 (m, 2H)		7.64 (bs)
7‴	7.61 (d, 16.0)	7.60 (d, 16.0)	7.91 (d, 16.0)	7.60 (d, 16.0)	7.89 (d, 16.0)	7.67 (d, 16.0)	7.92 (d, 16.0)	7.76 (d, 16.0)
8‴	6.40 (d, 16.0)	6.54 (d, 16.0)	6.74 (d, 16.0)	6.39 (d, 16.0)	6.72 (d, 16.0)	6.46 (d, 16.0)	6.74 (d, 16.0)	6.61 (d, 16.0)
3⁗–5⁗	7.35 **	-	-	7.34 **	7.57(bs)	-	-	-
2⁗, 6⁗	7.53 (d, 6.6)			7.51 (d, 6.1)	7.39 (d, 7.2)			
7⁗	7.70 (d, 16.0)	-	-	7.71 (d, 16.0)	7.99 (d, 16.0)	-	-	-
8⁗	6.50 (d, 16.0)	-	-	6.49 (d, 16.0)	6.80 (d, 16.0)	-	-	-

Table 1. *Cont.*

Pos.	1	2		3		4		7
	CD_3OD	DMSO d_6	Pyridine d_6	CD_3OD	Pyridine d_6	CD_3OD	Pyridine d_6	CD_3OD
Acetyl:								
6′	2.07 (s)	2.00 (s)	1.94 (s)	-	-	-	-	-
2″	2.19 (s)	2.02 (s)	2.06 (s)	2.19	2.10 (s)	2.06 (s)	2.07 (s)	
4″	-	2.13 (s)	2.11 (s)	-	-	2.18 (s)	2.10 (s)	

* Assignments based on DEPT135, COSY, HSQC, HMBC, H2BC, NOESY experiments and comparison with reported data. ** Overlapped signals.

Table 2. ^{13}C NMR data (δ ppm) for compounds 1–4 and **7** *.

Pos.	1 **	2 ***	3 **	4 **	7 **	Pos.	1 **	2 ***	3 **	4 **	7 **
1	93.95	94.03	93.82	93.76	93.83	3″	69.45	69.22	69.46	69.39	68.84
3	141.14	141.75	141.14	141.12	140.97	4″	71.05	70.70	71.07	70.90	74.15
4	102.06	102.46	101.95	101.80	102.09	5″	66.89	65.89	66.88	66.65	66.86
5	35.78	35.80	35.81	35.75	35.93	6″	16.53	17.62	16.54	16.35	16.54
6	83.74	83.21	83.61	83.47	82.77	1‴	134.00	134.11	133.97	134.07	134.32
7	58.02	57.56	58.14	58.07	58.13	2‴–6‴	128.01–130.45	129.01–131.26	128.00–130.43	128.04–130.46	127.95–130.26
8	65.08	66.62	65.21	65.19	65.25	7‴	146.28	146.07	146.26	146.04	145.39
9	41.85	42.14	41.92	41.87	41.91	8‴	116.50	117.41	116.51	116.47	117.42
10	60.17	59.22	60.07	60.01	60.06	9‴	165.93	165.75	165.92	165.89	166.98
1′	98.45	98.71	98.36	98.32	98.32	1⁗	134.00	-	133.97	-	-
2′	73.35	73.70	73.44	73.42	73.42	2⁗–6⁗	128.01–130.45	-	128.00–130.43	-	-
3′	76.02	76.51	76.28	76.27	76.25	7⁗	146.07	-	146.05	-	-
4′	70.06	70.26	70.37	70.37	70.35	8⁗	116.50	-	116.51	-	-
5′	74.36	74.22	77.22	77.22	77.19	9⁗	166.31	-	166.30	-	-
6′	62.74	63.27	61.58	61.55	61.52	Acetyl: 6′	19.54, 171.40	20.94, 170.72	-		-
1″	96.41	96.11	96.41	96.28	99.06	2″	19.48, 170.32	21.07, 170.23	19.49, 170.31	19.37, 170.30	-
2″	69.92	69.55	70.11	69.92	71.05	4″	-	21.04, 170.06	-	19.39, 170.53	-

* Assignments based on DEPT135, COSY, HSQC, HMBC, H2BC, NOESY experiments and comparison with reported data. ** Spectra measured in CD_3OD. *** Spectra measured in DMSO d_6.

HRESIMS data of **4** were consistent with the molecular formula $C_{34}H_{42}O_{17}$, as shown from the $[M+Na]^+$ at m/z of 745.2313, $[M+K]^+$ at m/z of 761.2051 and $[M-1]^-$ at m/z of 721.2355 (Figures S104 and S105). The absence of one acetyl group was clear in the NMR data and fully supported by the MS data (Figures S82–S89). In the spectra of **4**, the appearance of H-6′ and C-6′ of glucose at δ_H 3.65 (dd, J = 6.8, 12 Hz), 3.94 (d, J = 12 Hz) and δ_C 61.55 indicated that **4** is the C-6′ deacetylation derivative of **2**. Similar to **1**–**3**, the acylations in **4** were located at H-2″ (δ_H 5.88, s), H-3″ (δ_H 5.94, bd, J = 9.7 Hz) and H-4″ (δ_H 5.71, bd, J = 9.7 Hz) based on their downfield shift values. The *trans*-cinnamoyl moiety was assigned to position 3″ based on the HMBC correlation between H-3″ at δ_H 5.94 and the cinnamoyl carbonyl at δ_C 165.88 (Figures S92 and S93). Compound **4** was identified as 6-O-α-L(2″, 4″-diacetyl, 3″-O-*trans*-cinnamoyl) rhamnopyranosyl catalpol and was given the trivial name hypericifolioside B.

2.2. Biological Evaluation

The total extract of *S. hypericifolia* showed promising hepatoprotective and nephroprotective activities [20]. Compounds **2**–**4** and **6** isolated in good yield were subjected to biological testing against paracetamol (Pa)-induced liver and kidney toxicities. Toxic doses of Pa produce fatal hepatic necrosis in humans and other mammals, including rats and mice [37]. Toxic doses of Pa cause saturation of the sulfation and glucoronidation routes of metabolism. As an alternative to get rid of the extra Pa, the cytochrome P450 enzymes are enhanced to oxidize a higher percentage of Pa molecules to the highly reactive N-acetyl-p-benzoquinone imine (NAPQI) species. NAPQI's loss of one electron results in the formation of semi-quinone radicals with an extremely short half-life. It is then rapidly conjugated with the sulphydryl donor glutathione (GSH), resulting in the depletion of the liver GSH pool [38]. Excessive formation of NAPQI as well as glutathione store depletion leads to covalent binding of NAPQI to vital proteins and the lipid bilayer of hepatocyte membranes and enhances lipid peroxidation. These consequences lead to hepatocellular death and centrilobular liver necrosis [39]. The transport system of the hepatocytes was impaired, leading to the leakage of plasma membrane [40], reflected by increases in serum enzyme levels. Treatment of animals with Pa resulted in a dramatic elevation of transaminases (aspartate aminotransferase (AST), alanine aminotransferase (ALT)) and alkaline phosphatase (ALP) levels. Severe jaundice is expressed by the elevation of serum bilirubin levels (Figure 2 and Table S1) [41].

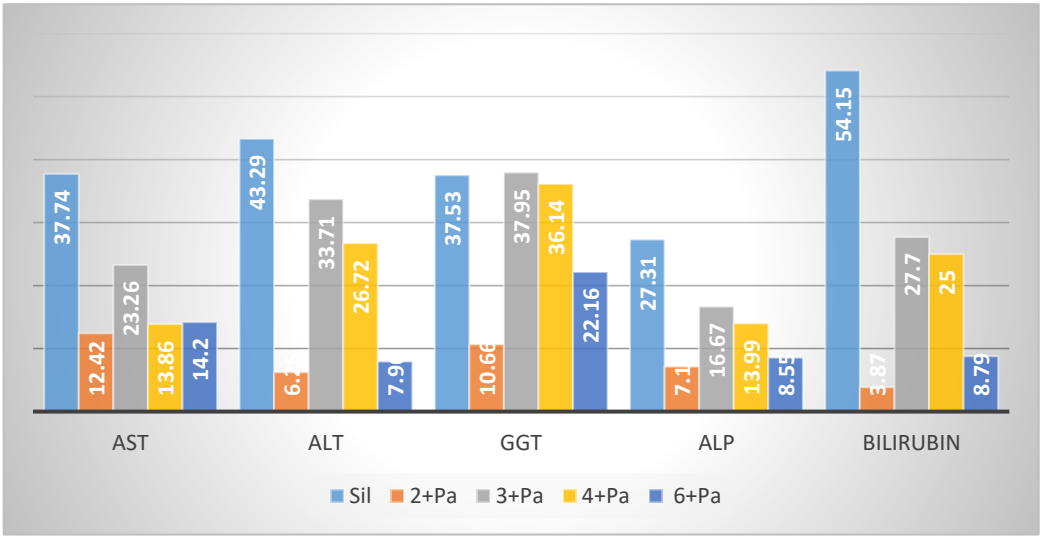

Figure 2. Effect of compounds **2**–**4**, **6** on liver serum biochemical parameters AST, ALT, GGT, APL and bilirubin (% reduction).

2.2.1. Hepatoprotective Effect

Administration of Sil, at a dose of 10 mg/kg (20.7 µmol/kg) prior to Pa resulted in a significant correction ($p < 0.001$) in the elevated AST (37.74%), ALT (43.29%), gamma glutamyl transpeptidase (GGT) (37.53%), ALP (27.31%) and bilirubin (54.15%) levels in the corresponding group of rats (Figure 2 and Table S1). Sil acts by several mechanisms including an antioxidant effect by scavenging prooxidant free radicals and via restoring the concentration of GSH. Sil also restores the normal cellular membrane function, resulting in protection against xenobiotic injury. Sil also initiates the synthesis of ribosomal RNA via activation of DNA polymerase-I and steroid-like action in regulating DNA transcription and enhancement of protein synthesis necessary for the regeneration of liver cells [42,43].

Treatment of rats with **3** at 20.7 µmol/kg doses prior to Pa showed a significant ($p <$ 0.01; 0.001) reduction by 23.26, 33.71, 37.95, 16.67 and 27.70% in the elevated levels of AST, ALT, GGT, ALP and bilirubin. Compound **4** showed less protection, expressed as 13.86, 26.72, 36.14, 13.99 and 25.00% reductions in the levels of AST, ALT, GGT, ALP and bilirubin. Compound **6** showed weaker effects on the serum biochemical parameters, while **2** was almost inactive (Figure 2). The impact of the tested compounds was also evaluated on total protein (TP) and non-protein sulfhydryl groups (NP-SH) levels in liver cells (Figure 3A, Figure 4 and Table S2). Compound **3** restored TP contents to about 50% of that of Sil. The effect of **3** restoring NP-SH (3.43 ± 0.30) was slightly less than the standard drug Sil (3.37 ± 0.28). The effects of **4** were less than **3**, followed by **6**. The results of the histopathological study were in support of the serum biochemical and tissue parameters obtained. Compared with the normal hepatocytes (Figure 5A), the liver samples of the group only treated with Pa (Figure 5B) showed severe damage, expressed as portal vessel congestion, necrosis and infiltration. The Sil-treated group indicated that Sil restores the liver cell architecture closer to the normal state (Figure 5C) with little congestion. The group treated with **3** expressed a great level of protection (Figure 5D) where the appearance of cells was almost normal. Mild focal necrosis and portal tract congestion were observed in the liver specimen of the group treated with **4** (Figure 5E), indicating a moderate level of protection. Less protection was evident from treatment with **6** as the cells suffered more from degeneration, portal congestion and inflammatory cell infiltration.

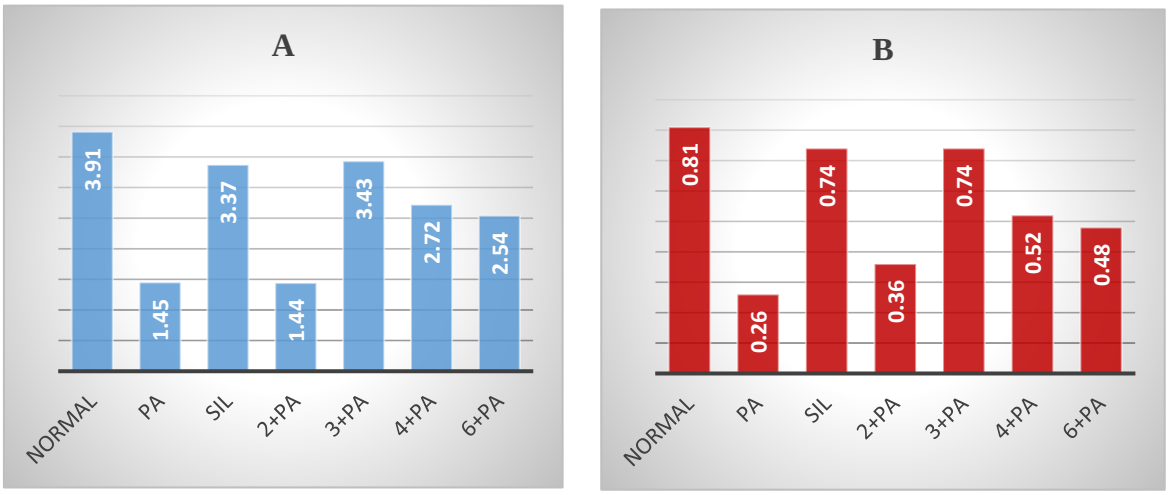

Figure 3. Effect of compounds **2**–**4**, **6** on liver (**A**) and kidney (**B**) TP.

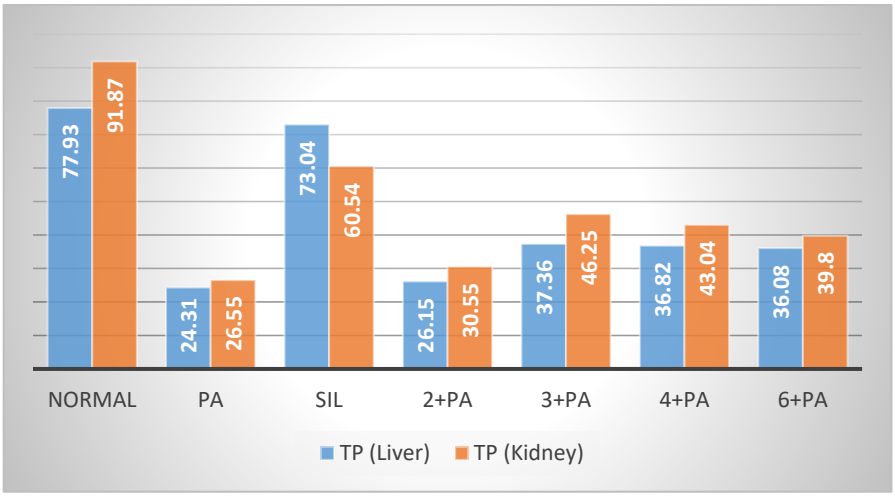

Figure 4. Effect of compounds **2**–**4**, **6** on liver and kidney NP-SH.

2.2.2. Nephroprotective Effect

The kidney is a vital organ responsible for the regulation of plasma ionic composition and the elimination of nitrogenous end metabolic waste products such as urea, creatinine and uric acid [44]. Elevations of these parameters are reliable parameters for nephrotoxicity [45]. Pa nephrotoxicity is reflected by elevated serum levels of creatinine, urea, sodium and potassium (Table S3). The levels of NP-SH and TP were diminished (Table S2). Treatment with Sil resulted in marked improvement of all these parameters. The group treated with **3** showed the most effective degree of protection among the tested compounds. Prior treatment with Sil resulted in a 39.87% reduction in urea, a 49.88% reduction in creatinine, a 57.46% reduction in sodium and a 46.03% reduction in potassium levels compared with 24.61%, 36.00%, 33.88% and 35.47% reductions in the same parameters, respectively, as a result of the administration of **3** (Figure 6, Table S3). Compound **3** was as effective as Sil in restoring NP-SH groups and slightly less in restoring TP (Figures 3B and 4, and Table S2). Less improvement was observed with treatment with **4**, followed by **6**, while **2** was totally ineffective. The normal kidney cells structure is presented in Figure 7A. Histopathological study revealed that the kidney cells of rats treated with Pa expressed severe changes (Figure 7B), such as degenerated corpuscle, reduced size of glomeruli, shrinkage of Bowman capsule, cloudy swelling in tubules and inflammatory infiltrate. Pre-administration of Sil (Figure 7C) resulted in nearly normal glomeruli and mild cloudy swelling in tubules, while the group treated with **3** (Figure 7D) expressed moderate cortical atrophy and moderate reduction in glomerular size. More damage was observed in groups treated with **4** (Figure 7E) and **6** (Figure 7F).

Many nutraceuticals containing well-known traditional plants are utilized for their liver and/or kidney health benefits. Extracts of *Nigella sativa* [46], *Chenopodium ambrosioides* [47], *Hemidesmus indicus* [48], *Bryophyllum pinnatum* [49] and *Verbascum thapsus* [50] are reported to have hepatoprotective and/or nephroprotective effects. Interestingly, *Verbascum thapsus* is rich in iridoid contents [50]. One of its components, the iridoid glycoside aucubin, was reported to have wide range of pharmacological activities, including hepatoprotective and antioxidant effects [51]. The hepatoprotective effects of related iridoid glycosides were reviewed [52]. Molecular docking analysis was performed to assess the binding efficiencies of iridoids to the active sites of human CYP3A4 enzyme. Selected iridoids were evaluated for their hepatoprotective effects using quantitative real-time PCR to measure the expression levels of CYP3A4 mRNA in HepG2 cells. The tested iridoids showed an inductive effect on CYP3A4 mRNA levels in the HepG2 cells. The study results indicated that the hepatoprotective effects were caused by the facilitation of drug metabolism and the reduction of both mitochondrial dysfunction and oxidative stress [53].

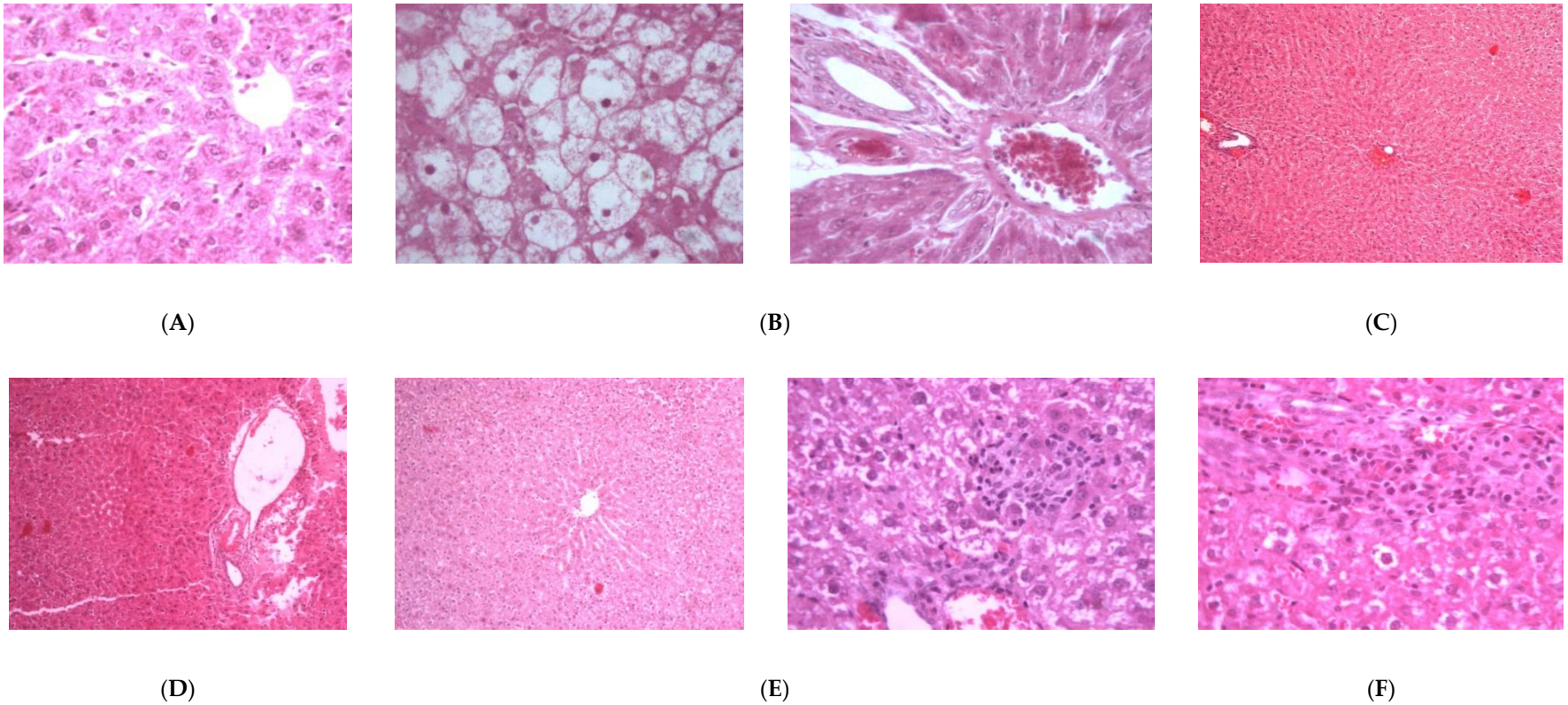

Figure 5. Light microscope pictures of liver tissues: (**A**) Liver cells of normal control group showing central vein, normal sinusoids and cells. (**B**) Liver cells of Pa-treated group showing hydropic swelling, rosette formation, portal dilated congested vessels, focal necrosis, lymphocytic infiltrate and lymphocytic exudate. (**C**) Liver cells of Pa- and Sil-treated group showing mostly normal cells with mild congestion in the central venules. (**D**) Liver cells of group treated with **3** showing almost normal lobules and portal tract with the absence of degeneration and vein congestion. (**E**) Liver cells of group treated with **4** showing mild focal necrosis and portal tract congestion. (**F**) Liver cells of group treated with **6** showing moderate to high degree of degeneration, portal congestion and inflammatory cell infiltration.

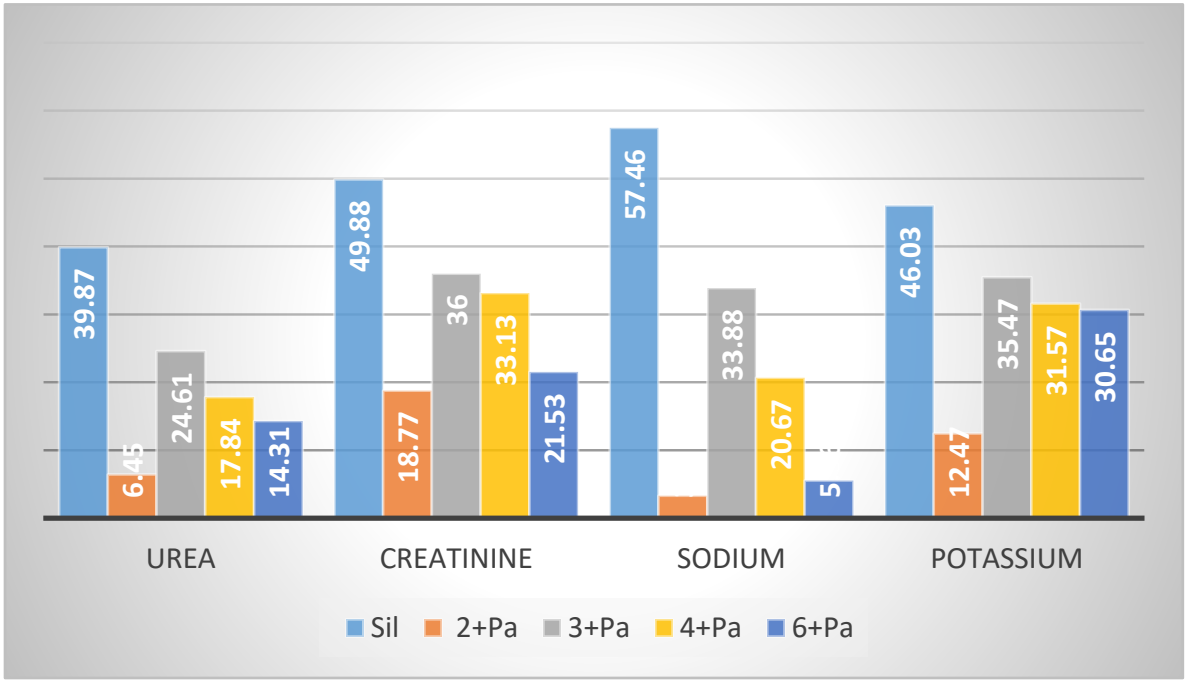

Figure 6. Effect of compounds **2**–**4**, **6** on kidney serum biochemical parameters (% reduction).

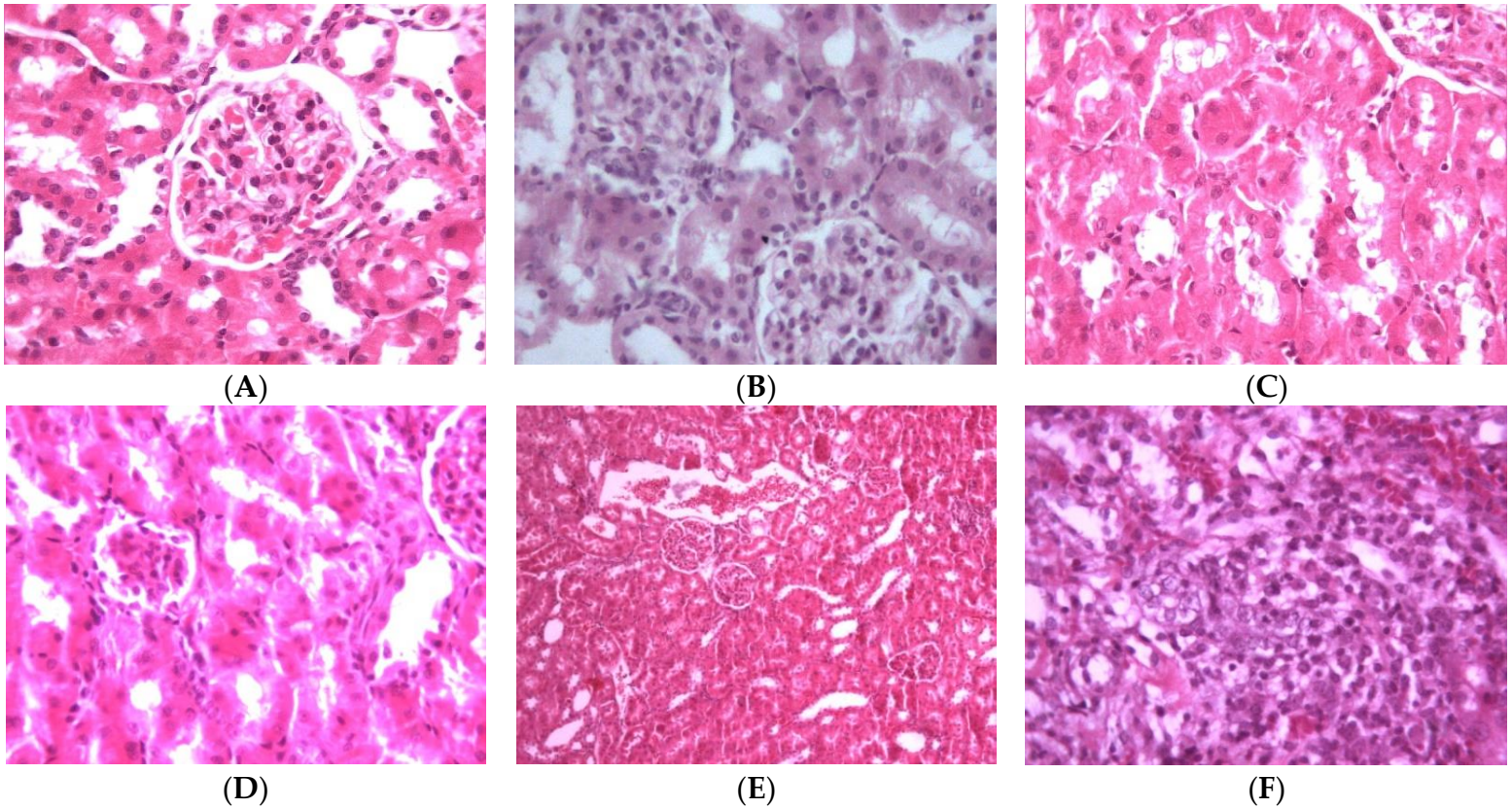

Figure 7. Light microscope pictures of kidney cells: (**A**) Normal cells. (**B**) Kidney cells of Pa-treated group showing abnormal cellular structures with degenerated corpuscle, reduced size of glomeruli, shrinkage of Bowman capsule, cloudy swelling in tubules and inflammatory infiltrate. (**C**) Kidney cells of rats treated with Pa and Sil showing no marked changes, nearly normal glomeruli and mild cloudy swelling in tubules. (**D**) Kidney cells of group treated with **3** showing moderate cortical atrophy and reduced size of glomeruli. (**E**) Kidney cells of group treated with **4** showing kidney cortical congestion, abnormal glomeruli (reduced in size) and cloudy swelling in tubules. (**F**) Kidney cells of group treated with **6** showing inflammatory cell infiltration at corticomedullary junction, kidney cortical infiltration, almost complete absence of Bowman space, degenerated and convoluted necrotic tubules.

3. Materials and Methods

3.1. General Experimental Procedures

Melting points were determined in open capillary tubes using a Thermosystem FP800 Mettler FP80 central processor supplied with an FP81 MBC cell apparatus and are shown uncorrected. Ultraviolet absorption spectra were measured on a Unicum Heyios a UV–Visible spectrophotometer. A Jasco P-2000 Polarimeter was used to measure the optical rotations. ^{1}H, ^{13}C-NMR and 2D-NMR data were measured on a Bruker UltraShield Plus 500 MHz spectrometer at NMR Unite, College of Pharmacy, Prince Sattam Bin Abdulaziz University, operated at 500 MHz for protons and 125 MHz for carbon atoms. Chemical shift values were reported in δ (ppm) relative to the residual solvent peaks. Coupling constants (*J*) are reported in Hertz (Hz). 2D-NMR experiments (COSY, HSQC, HMBC, H2BC, NOESY and/or ROESY) were performed utilizing the standard Bruker program. HRMS were determined by direct injection using a Thermo Scientific UPLC RS Ultimate 3000 Q Exactive hybrid quadrupole—Orbitrap mass spectrometer combining high-performance quadrupole precursor selection with high-resolution, accurate mass (HR/AM) Orbitrap™ detection. Direct infusion of isocratic elution acetonitrile/methanol (70:30) with 0.1% formic acid was used to flush the samples. Runtime was 1 min using nitrogen as auxiliary gas with a flow rate of 5 µL/min. A scan range from 160–1500 m/z was used. Resolving power was adjusted to 70,000 @ m/z 200. Detection was in both positive and negative modes separately. Calibration was done using Thermo Scientific Pierce™ LTQ Velos ESI Positive Ion Calibration Solution including caffeine, Met-Arg-Phe-Ala (MRFA), Ultramark 1621, n-Butyl-amine components and Pierce™ LTQ Velos ESI Negative Ion Calibration Solution including sodium dodecyl sulphate (SDS), sodium taurocholate and Ultramark 1621 components. The capillary temperature was set at 320 °C and capillary voltage at 4.2 Kv. A Sephadex LH-20 (Amersham Biosciences, Uppsala, Sweden), silica gel 60/230–400 mesh (EM Science) and RP18 silica gel 40–63/230–400 mesh (Fluka) were used for column chromatography. Centrifugal preparative thin layer chromatography (CPTLC) using a 2 mm silica gel P254 disc was performed on a Chromatotron (Harrison Research Inc. model 7924, San Bruno, CA, USA). The thin layer chromatography (TLC) analysis was performed on Kiesel gel 60 F254 and RP-18 F254S (Merck) plates. A UV lamp (entela Model UVGL-25) operated at 254 nm was used for detecting spots on the TLC plates.

3.2. Plant Material

The plants of *Scrophularia hypericifolia* Wydler (aerial parts) were described earlier [20] and collected in March, 2019 from Al-Qassim Province, Saudi Arabia. The plants were identical to the voucher specimen (# 13274) preserved at the herbarium of the Medicinal, Aromatic and Poisonous Plants Research Center (MAPPRC).

3.3. Extraction and Isolation

Air-dried powdered aerial parts (1000 g) were repeatedly extracted with 95% ethanol by percolation at room temperature till exhaustion. The solvent was distilled off under reduced pressure using a rotary vacuum evaporator at 40 °C to give 130 g residue. Part of the obtained dried extract (35 g) was dissolved in 800 mL of 40% aqueous ethanol and fractionated with light petroleum (500 mL × 3) to yield 9.25 g of light petroleum-soluble fraction, chloroform (500 mL × 4) to yield 15.32 g of chloroform-soluble fraction and n-butanol (400 mL × 2) to yield 3.15 g of n-butanol-soluble fraction.

The chloroform-soluble fraction was fractionated chromatographically using a silica gel column (150 × 7 cm i.d., 450 g) eluting with chloroform, followed by chloroform/methanol mixtures with a gradual increase in methanol content. Fractions of 200 mL each were collected, screened by TLC and similar fractions were pooled to yield 6 major fractions (A–F). Fraction A (1.51 g) eluted with 5% methanol in chloroform was further purified using an RP18 column (45 × 2 cm i.d., 40 g) eluting with 20% water in methanol to afford 85 mg of **1** and 328 mg of **2** after crystallization from methanol. Fraction B (0.93 g) eluted with 10% methanol in chloroform afforded 325 mg of **3** after purification on an RP18

column (45 × 2 cm i.d., 30 g) eluting with 20% water in methanol. Fraction C (2.73 g) eluted with 10% methanol in chloroform was chromatographed on an RP18 column (90 × 2.5 cm i.d., 90 g) eluting with 20% water in methanol to afford another 200 mg of **3**. Further purification on a Sephadex LH20 eluting with 10% water in methanol afforded 272 mg of **4** from fractions 4–7. Fractions 11–14 were further purified using a Chromatotron equipped with 2 mm silica gel plates and 2% methanol in acetonitrile as the mobile phase to afford 17 mg of cinnamic acid and 92 mg of **5**. Fraction D (1.43 g) eluted with 10% methanol in chloroform was chromatographed on an RP18 column (90 × 2.5 cm i.d., 45 g) eluting with 20% water in methanol to afford 439 mg of **6**. Fraction E (0.67 g) eluted with 20% methanol in chloroform was further purified on a Sephadex LH20 eluting with 20% water in methanol followed by separation on a Chromatotron equipped with 2 mm silica gel plates and 15% methanol in chloroform to afford 32 mg of **7** and 58 mg of **8**. Fraction F (0.43 g) eluted with 20% methanol in chloroform was chromatographed on an RP18 column (45 × 2 cm i.d., 90 g) eluting with 30% water in methanol to afford another 130 mg of **9**.

3.4. Compound Characterization

3.4.1. 6′-Acetyl hypericifolioside A (1)

White powder; m.p. 120.8 °C, $[\alpha]_{25}^{D}$ -58; UV λ_{max} MeOH: 220, 302, 325 nm; ^{1}H and ^{13}C NMR see Tables 1 and 2; HRESIMS $[M+Na]^+$ m/z 875.2733 (calcd for $C_{43}H_{48}O_{18}Na$, 875.2733), $[M+K]^+$ m/z 891.2471 (calcd for $C_{43}H_{48}O_{18}K$, 891.2478).

3.4.2. 6′-Acetyl hypericifolioside B (2)

White powder; m.p. 126.9 °C, $[\alpha]_{25}^{D}$ -155; UV λ_{max} MeOH: 218, 301, 326 nm; ^{1}H and ^{13}C NMR see Tables 1 and 2; HRESIMS $[M+Na]^+$ m/z 787.2412 (calcd for $C_{36}H_{44}O_{18}Na$, 787.2425), $[M-1]^-$ m/z 763.2454 (calcd for $C_{36}H_{43}O_{18}$, 763.2449).

3.4.3. Hypericifolioside A (3)

White powder; m.p. 138.0 °C, $[\alpha]_{25}^{D}$ -56; UV λ_{max} MeOH: 220, 300, 326 nm; ^{1}H and ^{13}C NMR see Tables 1 and 2; HRESIMS $[M+Na]^+$ m/z 833.2616 (calcd for $C_{41}H_{46}O_{17}Na$, 833.2633), $[M+K]^+$ m/z 849.2348 (calcd for $C_{41}H_{46}O_{17}K$, 849.2372).

3.4.4. Hypericifolioside B (4)

White powder; m.p. 133.4 °C, $[\alpha]_{25}^{D}$ -154; UV λ_{max} MeOH: 221, 301, 325 nm; ^{1}H and ^{13}C NMR see Tables 1 and 2; HRESIMS $[M+Na]^+$ m/z 745.2313 (calcd for $C_{34}H_{42}O_{17}Na$, 745.2320), $[M+K]^+$ m/z 761.2051 (calcd for $C_{34}H_{42}O_{17}k$, 761.2059), $[M-1]^-$ m/z 721.2355 (calcd for $C_{34}H_{41}O_{17}$, 721.2344).

3.5. Animals

Male Wistar albino rats of average weight (160–180 g) (age 8–10 weeks) were secured by the Experimental Animal Care Center, College of Pharmacy, Prince Sattam Bin Abdulaziz University, Al-Kharj, KSA. The animals were kept under controlled conditions of temperature (22 ± 2 °C), humidity (55%) and light/dark cycle (12/12 h). The animals were provided with Purina chow and free access to drinking water ad libitum [20]. The experimental protocol was approved by the Bioethical Research Committee at Prince Sattam Bin Abdulaziz University.

3.6. Hepatoprotective and Nephroprotective Activity

Rats were divided into seven groups of five animals. Group 1 was designated as the control group and received normal saline only. Groups 2–7 received Pa via the intraperitoneal route for two days at 500 mg/kg body weight. Group 2 did not receive any further treatment. Group 3 was treated with 10 mg/kg p.o. (20.7 µmol/kg) of Sil (Sigma-Aldrich, St. Louis, MO, USA) [20]. Groups 4–7 were treated with 20.7 µmole/kg body weight of compounds **2**–**4**, **6**. Treatment started 5 days prior to Pa administration and continued to the end of the experimental protocol. After 24 h, following the second dose of Pa, the

animals were sacrificed using ether anesthesia. Blood samples were collected by heart puncture and the serum was separated to estimate the biochemical parameters. The liver and kidney tissues were immediately removed and properly treated for the determination of the tissue parameters. Representative pieces were immersed in 10% formalin for fixation to carry out the histopathological study.

3.7. Determination of Biochemical Serum Parameters

Serum glutamate oxaloacetate transaminase (AST), serum glutamate pyruvate transaminase (ALT), gamma glutamyltranspeptidase (GGT), alkaline phosphatase (ALP) and total bilirubin were determined following the reported methods [54]. The enzyme activities were measured by Reflotron® diagnostic strips (Roche, Basel, Switzerland) and a Reflotron® Plus instrument (Roche) (Figure 2 and Table S1).

Serum creatinine and blood urea were assayed using Randox Diagnostic kits (Randox Laboratories Ltd., Crumlin, U.K.) by the reported method [55]. Potassium levels were measured using diagnostic strips (Reflotron®, Roche), while sodium levels were determined photometrically using the Mg-uranyl acetate method (Figure 3 and Table S2) [56].

3.8. Determination of Non-Protein Sulfhydryl Groups and Total Protein

The liver and kidney tissues were homogenized in 0.02 M EDTA using a Potter–Elvehjem type C homogenizer (Sigma-Aldrich, St. Louis, MO, USA). Homogenates equivalent to 100 mg of tissues were used for the measurements. Nonprotein sulfhydryl groups (NP-SH) were quantified by dilution of the homogenates with 4 mL of distilled water and 1 mL of 50% trichloroacetic acid (TCA) followed by shaking for 15 min. The supernatants were then mixed with 2 mL Tris buffer, pH 8.9 and 0.1 mL of 0.01 M of 5,5′-dithio-bis-(2-nitrobenzoic acid) (DTNB). The absorbances were measured spectrophotometrically within 5 min at 412 nm against a reagent blank with no homogenate (Figure 4 and Table S3) [57]. TP were quantified by mixing homogenates with 0.7 mL of Lowry's solution followed by incubation in the dark for 20 min at room temperature. Diluted Folin's reagent (0.1 mL) was then added, and samples were incubated at room temperature in the dark for 30 min. The absorbances were then measured at 750 nm (Figure 5 and Table S3) [58].

3.9. Statistical Analysis

An analysis of variance (ANOVA) test was used to evaluate the significance of the difference between the groups. Non-paired samples such as the control and Pa-treated group were compared for significance using Dunnett's test [59]. All the reported values are presented as mean ± S.E.

3.10. Histopathology

Water-ethanol mixtures with a gradual increase in ethanol were used to dehydrate liver and kidney samples till reaching absolute ethanol, cleared and infiltrated by immersion in increasing concentrations of ethanol (70–100%) and xylene (3 times, 1 h each) followed by paraffin wax (4 times, 1 h each). The tissues were placed by hot forceps in molds, chilled on cold plates and excess waxes were removed. Thin sections of 3 µm were obtained by a rotary microtome (Leitz 1512) and placed onto clean slides. The slides were drained and stained using Mayer's hematoxylin solution for 15 min after deparaffinization and hydration. The slides were then washed in lukewarm tap water for 15 min then immersed in 80% ethanol for two minutes and counterstained in eosin-phloxine solution for 2 min. The slides were then washed with 95% ethanol, absolute ethanol and xylene (2 min each) and finally mounted in resinous medium [60].

4. Conclusions

A phytochemical study of the aerial parts of *Scrophularia hypericifolia* resulted in the isolation of nine acylate iridoid glycosides. Four new compounds were identified as 6′-acetyl hypericifolioside A (**1**) 6′-acetyl hypericifolioside B (**2**) hypericifolioside A

(**3**) and hypericifolioside B (**4**). In addition, five known compounds were identified as laterioside (**5**) 8-O-acetylharpagide (**6**) 6-O-L(4″-O-*trans*-cinnamoyl) rhamnopyranosyl catalpol (**7**) lagotisoside D (**8**) and harpagoside (**9**). Compounds **2**–**4** and **6** were tested against paracetamol-induced hepatic and renal toxicity. Compound **3** resulted in 23.26, 33.71, 37.95, 16.67 and 27.70% reductions in the elevated levels of AST, ALT, GGT, ALP and bilirubin. It also reduced the levels of urea, creatinine, sodium and potassium by 24.61%, 36.00%, 33.88% and 35.47%, respectively. Compound **3** restored TP contents and NP-SH in both liver and kidney tissues to levels comparable to Sil. These findings were supported by histopathological study by the almost normal appearance of liver cells, while little degeneration was observed in kidney cells after treatment with **3**. In some of the measured parameters, **3** was as protective as the standard drug Sil. Compounds **4** and **6** expressed less protection, while **2** was almost inactive.

Supplementary Materials: The following are available online at https://www.mdpi.com/2079-7737/10/2/145/s1.

Author Contributions: Conceptualization, M.S.A.-K. and S.I.A.; methodology, M.S.A.-K. and S.I.A.; validation, M.S.A.-K. and S.I.A.; investigation, M.S.A.-K. and S.I.A.; resources, M.S.A.-K. and S.I.A.; data curation, M.S.A.-K.; writing—original draft preparation, S.I.A.; writing—review and editing, M.S.A.-K.; visualization, M.S.A.-K. and S.I.A.; supervision, M.S.A.-K. The two authors have read and agreed to the published version of the manuscript.

Funding: This research received no external funding.

Institutional Review Board Statement: The study was conducted according to the guidelines of the Declaration of Helsinki, and approved by the Bioethical Research Committee at Prince Sattam Bin Abdulaziz University (Approval no. BERC-003-12-19, 12-12-2019).

Informed Consent Statement: Not applicable.

Data Availability Statement: The data presented in this study are available in Supplementary Figures and Tables.

Acknowledgments: The authors are thankful to the Deanship of Scientific Research (DSR), Prince Sattam bin Abdulaziz University, Al-Kharj, Saudi Arabia. Our thanks are also due to A. Hamad, College of Applied Medical Science at Prince Sattam University for the histopathological study.

Conflicts of Interest: The authors declare no conflict of interest.

References

1. Scheunert, A.; Heubl, G. Phylogenetic relationships among New World *Scrophularia* L. (Scrophulariaceae): New insights inferred from DNA sequence data. *Plant Syst. Ecol.* **2011**, *291*, 69–89. [CrossRef]
2. Collenette, S. *Wild Flowers of Saudi Arabia*; East Anglian Engraving, Co.: Norwich, UK, 1999.
3. Flora of Saudi Arabia-Checklist. Available online: http://plantdiversityofsaudiarabia.info/Biodiversity-Saudi-Arabia/Flora/Checklist/Cheklist.htm (accessed on 9 February 2021).
4. Zhu, Y.P. *Chinese Materia Medica: Chemistry, Pharmacology and Applications*; Amsterdam Harwood Academic Publishers: Amsterdam, The Netherlands, 1998.
5. Marty, A.T. The complete German commission E monographs: Therapeutic guide to herbal medicines. *JAMA* **1999**, *281*, 1852–1853. [CrossRef]
6. Guarrera, P.M.; Lucia, L.M. Ethnobotanical remarks on central and southern Italy. *J. Ethnobiol. Ethnomed.* **2007**, *3*, 23. [CrossRef] [PubMed]
7. Pieroni, A.; Quave, C.L.; Santoro, R.F. Folk pharmaceutical knowledge in the territory of the Dolomiti Lucane, inland southern Italy. *J. Ethnopharmacol.* **2004**, *95*, 373–384. [CrossRef] [PubMed]
8. Pasdaran, A.; Delazar, A.; Nazemiyeh, H.; Nahar, L.; Sarker, S.D. Chemical composition, and antibacterial (against *Staphylococcus aureus*) and free radical-scavenging activities of the essential oils of *Scrophularia amplexicaulis* Benth. *Rec. Nat. Prod.* **2012**, *6*, 350–355.
9. Ahmed, B.; Al-Rehaily, A.J.; Al-Howiriny, T.A.; El-Sayed, K.A.; Ahmad, M.S. Scropolioside-D2 and harpagoside-B: Two new iridoid glycosides from *Scrophularia deserti* and their antidiabetic and antiinflammatory activity. *Biol. Pharm. Bull.* **2003**, *26*, 462–467. [CrossRef]
10. Zhu, L.J.; Hou, Y.L.; Shen, X.Y.; Pan, X.D.; Zhang, X.; Yao, X.S. Monoterpene pyridine alkaloids and phenolics from *Scrophularia ningpoensis* and their cardioprotective effect. *Fitoterapia* **2013**, *88*, 44–49. [CrossRef] [PubMed]

11. Lee, E.; Kim, S.; Kim, J.; Kim, Y. Hepatoprotective phenylpropanoids from *Scrophularia buergeriana* roots against CCl_4-induced toxicity: Action mechanism and structure–activity relationship. *Planta Med.* **2003**, *68*, 407–411. [CrossRef]
12. Garg, H.; Bhandari, S.; Tripathi, S.; Patnaik, G.; Puri, A.; Saxena, R.; Saxena, R. Antihepatotoxic and immunostimulant properties of iridoid glycosides of *Scrophularia koelzii*. *Phytother. Res.* **1994**, *8*, 224–228. [CrossRef]
13. Stevenson, P.C.; Simmonds, M.S.; Sampson, J.; Houghton, P.J.; Grice, P. Wound healing activity of acylated iridoid glycosides from *Scrophularia nodosa*. *Phytother. Res.* **2002**, *16*, 33–35. [CrossRef]
14. Germinara, G.S.; Frontera, A.M.; De Cristofaro, A.; Rotundo, G. Insecticidal activity of different extracts from *Scrophularia canina* L. against *Culex pipiens* molestus Forskal (Diptera, Culicidae). *J. Environ. Sci. Health B* **2011**, *46*, 473–479. [PubMed]
15. Han, M.-F.; Zhang, X.; Zhang, L.-Q.; Li, Y.-M. Iridoid and phenylethanol glycosides from *Scrophularia umbrosa* with inhibitory activity on nitric oxide production. *Phytochem. Lett.* **2018**, *28*, 37–41. [CrossRef]
16. Renda, G.; Korkmaz, B.; Kılıç, M.; Duman, M.K.; Kırmızıbekmez, H. Evaluation of in vivo analgesic activity of *Scrophularia kotscyhana* and isolation of bioactive compounds through activity-guided fractionation. *Nat. Prod. Res.* **2018**, *32*, 1902–1910. [CrossRef] [PubMed]
17. GBD 2017 Cirrhosis Collaborators. The global, regional, and national burden of cirrhosis by cause in 195 countries and territories, 1990–2017: A systematic analysis for the Global Burden of Disease Study 2017. *Lancet Gastroenterol. Hepatol.* **2020**, *5*, 245–266. [CrossRef]
18. Townsend, S.A.; Newsome, P.N. Non-alcoholic fatty liver disease in 2016. *Br. Med. Bull.* **2016**, *119*, 43–56. [CrossRef]
19. Cicero, A.F.G.; Colletti, A.; Bellentani, S. Nutraceutical approach to non-alcoholic fatty liver disease (NAFLD): The available clinical evidence. *Nutrients* **2018**, *10*, 1153. [CrossRef]
20. Alqasoumi, S.I. Evaluation of the hepatroprotective and nephroprotective activities of *Scrophularia hypericifolia* growing in Saudi Arabia. *Saudi Pharma. J.* **2014**, *22*, 258–263. [CrossRef] [PubMed]
21. Swiatek, L.; Lehmann, D.; Sticher, O. Iridoid glycosides of *Scrophularia lateriflora* Trautv. (Scrophulariaceae). *Pharm. Acta Helv.* **1981**, *56*, 37–44.
22. Stavri, M.; Mathew, K.T.; Gibbons, S. Antimicrobial constituents of *Scrophularia deserti*. *Phytochemistry* **2006**, *67*, 1530–1533. [CrossRef]
23. Nykmukanova, M.M.; Eskalieva, B.K.; Burasheva, G.S.; Iqbal Choudhary, M.; Adhikari, A.; Amadou, D. Iridoids from *Verbascum marschallianum*. *Chem. Nat. Compd.* **2017**, *53*, 580–581. [CrossRef]
24. Brownstein, K.J.; Gargouri, M.; Folk, W.R.; Gang, D.R. Iridoid and phenylethanoid/phenylpropanoid metabolite profiles of *Scrophularia* and *Verbascum* species used medicinally in North America. *Metabolomics* **2017**, *13*, 133. [CrossRef]
25. Ganaie, H.A.; Ali, M.N.; Ganai, B.A.; Meraj, M.; Ahmad, M. Antibacterial activity of 14, 15-dihydroajugapitin and 8-o-acetylharpagide isolated from *Ajuga bracteosa* Wall ex. Benth against human pathogenic bacteria. *Microb. Pathog.* **2017**, *103*, 114–118. [CrossRef]
26. You, Y.; Wang, J.; Tong, Y.; Hao, Q.; Li, Y.; Yang, H.; Huang, L.; Liao, F. Anti-inflammatory effect of acetylharpagide demonstrated by its influence on leukocyte adhesion and transmigration in endothelial cells under controlled shear stress. *Clin. Hemorheol. Microcirc.* **2014**, *56*, 205–217. [CrossRef]
27. Breschi, M.C.; Martinotti, E.; Catalano, S.; Flamini, G.; Morelli, I.; Pagni, A.M. Vasoconstrictor activity of 8-O-acetylharpagide from *Ajuga reptans*. *J. Nat. Prod.* **1992**, *55*, 1145–1148. [CrossRef]
28. Konoshima, T.; Takasaki, M.; Tokuda, H.; Nishino, H. Cancer chemopreventive activity of an iridoid glycoside, 8-acetylharpagide, from *Ajuga decumbens*. *Cancer Lett.* **2000**, *157*, 87–92. [CrossRef]
29. Kawamura, F.; Ohara, S. Antifungal activity of iridoid glycosides from the heartwood of *Gmelina arborea*. *Holzforschung* **2005**, *59*, 153–155. [CrossRef]
30. Al Ati, H.Y.; Fawzy, G.A.; El Gamal, A.A.; Khalil, A.T.; El Tahir, K.; Abdel-Kader, M.S.; Gilani, A.H. Phytochemical and biological evaluation of *Buddleja polystachya* growing in Saudi Arabia. *Pak. J. Pharm. Sci.* **2015**, *28*, 1533–1540. [PubMed]
31. Yang, X.D.; Yang, L.J.; Yang, S.; Zhao, J.F.; Zhang, H.B.; Li, L. Two new iridoid glycosides from *Lagotis yunnanensis*. *Z Nat. B* **2007**, *62*, 749–752.
32. Zhang, L.; Zhu, T.; Qian, F.; Xu, J.; Dorje, G.; Zhao, Z.; Guo, F.; Li, Y. Iridoid glycosides isolated from *Scrophularia dentata* Royle ex Benth. and their anti-inflammatory activity. *Fitoterapia* **2014**, *98*, 84–90. [CrossRef] [PubMed]
33. Li, Y.M.; Jiang, S.H.; Gao, W.Y.; Zhu, D.Y. Iridoid glycosides from *Scrophularia ningpoensis*. *Phytochemistry* **1999**, *50*, 101–104. [CrossRef]
34. Tunmann, P.; Lux, R. Zur Kenntniss der Inhaltsstoffe aus der Wurzel von H.p Dtsch. *Apoth. Ztg.* **1962**, *102*, 1274–1275.
35. Firestein, G.S. Evolving concepts of rheumatoid arthritis. *Nature* **2003**, *423*, 356–361. [CrossRef]
36. Saracoglu, I.; Oztunca, F.H.; Nagatsu, A.; Harput, U.S. Iridoid content and biological activities of *Veronica cuneifolia* subsp. cuneifolia and *V. cymbalaria*. *Pharm. Biol.* **2011**, *49*, 1150–1157. [CrossRef] [PubMed]
37. Mitchell, J.R.; Jollow, D.J.; Potter, W.Z.; Gillete, J.R.; Brrodle, B.N. Acetaminophen induced hepatic necrosis. I. Role of drug metabolism. *J. Pharmacol. Exp. Ther.* **1973**, *187*, 185–194. [PubMed]
38. Remirez, D.; Commandeur, J.N.M.; Ed Groot, E.; Vermeulen, P.E. Mechanism of protection of Lobenzarti against paracetamol-induced toxicity in rat hepatocytes. *Eur. J. Pharmacol.* **1995**, *293*, 301–308. [CrossRef]

39. McConnachie, L.A.; Mohar, I.; Hudson, F.N.; Ware, C.B.; Ladiges, W.C.; Fernandez, C.; Chatterton-Kirchmeier, S.; White, C.C.; Pierce, R.H.; Kavanagh, T.J. Glutamate cysteine ligase modifier subunit deficiency and gender as determinants of acetaminophen-induced hepatotoxicity in mice. *Toxicol. Sci.* **2007**, *99*, 628–636. [CrossRef]
40. Zimmerman, H.J.; Seeff, L.B. Enzymes in hepatic disease. In *Diagnostic Enzymology*; Goodly, E.I., Ed.; Lea and Febiger: Philadelphia, PA, USA, 1970.
41. Lin, C.C.; Shieh, D.E.; Yen, M.N. Hepatoprotective effects of fractions Ban-zhi-lian of experimental liver injuries in rats. *J. Ethnopharmacol.* **1997**, *56*, 193–200. [CrossRef]
42. Dehmlow, C.; Murawski, N.; de Groot, H. Scavenging of reactive oxygen species and inhibition of arachidonic acid metabolism by silybinin in human cells. *Life Sci.* **1996**, *52*, 1591–1600. [CrossRef]
43. Saller, R.; Melzer, J.; Rechling, J.; Brignoli, R.; Meier, R. An updated systematic review of the pharmacology of silymarin. *Forschende Komplementärmedizin* **2007**, *14*, 70–80. [CrossRef]
44. Pocock, G.; Richards, C.D. *Human Physiology: The Basis of Medicine*, 3rd ed.; Oxford University Press: Oxford, UK, 2006.
45. Adelman, R.D.; Spangler, W.L.; Beasom, F.; Ishizaki, G.; Conzelman, G.M. Frusemide enhancement of neltimicin nephrotoxicity in dogs. *J. Antimicrob. Chemother.* **1981**, *7*, 431–435. [CrossRef]
46. Adam, G.O.; Rahman, M.M.; Lee, S.-J.; Kim, G.-B.; Kang, H.-S.; Kim, J.-S.; Kim, S.-J. Hepatoprotective effects of Nigella sativa seed extract against acetaminophen-induced oxidative stress. *Asian Pac. J. Trop. Med.* **2016**, *9*, 221–227. [CrossRef]
47. Ogunleyea, G.S.; Fagbohunb, O.F.; Babalola, O.O. *Chenopodium ambrosioides* var. ambrosioides leaf extracts possess regenerative and ameliorative effects against mercury-induced hepatotoxicity and nephrotoxicity. *Ind. Crops Prod.* **2020**, *154*, 112723. [CrossRef]
48. Nandy, S.; Mukherjee, A.; Pandey, D.K.; Ray, P.; Dey, A. Indian Sarsaparilla (*Hemidesmus indicus*): Recent progress in research on ethnobotany, phytochemistry and pharmacology. *J. Ethnopharmacol.* **2020**, *254*, 112609. [CrossRef]
49. Latif, A.; Ashiq, K.; Qayyum, M.; Ashiq, S.; Ali, E.; Anwer, I. Phytochemical and pharmacological profile of the medicinal herb: *Bryophyllum pinnatum*. *J. Anim. Plant Sci.* **2019**, *29*, 1528–1534.
50. Panchal, M.A.; Murti, K.; Lambole, V. Pharmacological properties of *Verbascum Thapsus*—A review. *Int. J. Pharm. Sci. Rev. Res.* **2010**, *5*, 15.
51. Zeng, X.; Guo, F.; Ouyang, D. A review of the pharmacology and toxicology of aucubin. *Fitoterapia* **2020**, *140*, 104443. [CrossRef]
52. Wang, C.; Gong, X.; Bo, A.; Zhang, L.; Zhang, M.; Zang, E.; Zhang, C.; Li, M. Iridoids: Research Advances in Their Phytochemistry, Biological Activities, and Pharmacokinetics. *Molecules* **2020**, *25*, 287. [CrossRef]
53. Dai, K.; Yi, X.-J.; Huang, X.-J.; Muhammad, A.; Li, M.; Li, J.; Yanga, G.-Z.; Gao, Y. Hepatoprotective activity of iridoids, seco-iridoids and analog glycosides from Gentianaceae on HepG2 cells via CYP3A4 induction and mitochondrial pathway. *Food Funct.* **2018**, *9*, 2673. [CrossRef]
54. Edwards, C.R.W.; Bouchier, I.A.D. *Davidson's Principles and Practice Medicine*; Churchill Livingstone Press: London, UK, 1991.
55. Varley, H.; Alan, H.G. Tests in renal disease. In *Practical Clinical Biochemistry*; William Heinemann Medical Book Ltd.: London, UK, 1984; Volume 1123.
56. Henry, R.J.; Cannon, D.C.; Winkelman, J.W. *Clinical Chemistry, Principles and Techniques*, 2nd ed.; Harper Row: New York, NY, USA, 1974.
57. Sedlak, J.; Lindsay, R.H. Estimation of total, protein-bound, and nonprotein sulfhydryl groups in tissue with Ellman's reagent. *Anal. Biochem.* **1968**, *25*, 192–205. [CrossRef]
58. Lowry, O.H.; Rosebrough, N.J.; Farr, A.L.; Randall, R.J. Protein measurement with the Folin-phenol reagent. *J. Biol. Chem.* **1951**, *193*, 265–275. [CrossRef]
59. Woolson, R.F.; Clarke, W.R. *Statistical Methods for the Analysis of Biomedical Data*, 2nd ed.; John Wiley & Sons. Inc.: New York, NY, USA, 2002.
60. Prophet, E.P.; Mills, B.; Arrington, J.B.; Sobin, L.H. *Laboratory Methods in Histology*, 2nd ed.; American Registry of Pathology: Washington, DC, USA, 1994.